Journal of Electrochemistry

Manuscript 3446

In situ diffuse reflectance spectroelectrochemistry of cathode materials in lithium-ion batteries

Author #1

Author #2

Author #3

Author #4

ARTICLE

Invited Contribution from Award Winners of the 21st National Electrochemistry Congress in 2023

In situ Diffuse Reflectance Spectroelectrochemistry of Cathode Materials in Lithium-ion Batteries

Lu-Lu Chen, Hao-Ran Li*, Wei-Yi Liu, Wei Wang*

State Key Laboratory of Analytical Chemistry for Life Science, School of Chemistry and Chemical Engineering, Nanjing University, Nanjing 210023, China

Abstract

Developing *in situ* spectroelectrochemistry methods, which can provide detailed information about species transformation during electrochemical reactions, is very important for studying electrode reaction mechanisms and improving battery performance. Studying real-time changes in the surface of electrode materials during normal operation can be an effective way to assess and optimize the practical performance of electrode materials, thus, *in situ* and *in operando* characterization techniques are particularly important. However, batteries are hard to be studied by *in situ* characterization measurements due to their hermetically sealed shells, and there is still much room for battery characterizations. In this work, a specially designed battery based on the structure of coin cells, whose upper cover was transparent, was constructed. With such a device, acquisition of diffuse reflectance spectra of electrode materials during charging and discharging was realized. This not only provided a simple measurement accessory for diffuse reflectance spectroscopy (DRS), but also complemented *in situ* characterization techniques for batteries. Taking commonly used cathode materials in lithium-ion batteries (LIBs), including $LiFePO_4$ (LFP), NCM811 and $LiCoO_2$ (LCO) as examples, we managed to find out the response relationships of different electrode materials to visible light of different wavelengths under ordinary reflectance illumination conditions. Heterogeneity of different cathode materials on interaction relationships with the lights of different wavelengths was also revealed. This work demonstrated the capability of guiding wavelength selection for different materials and assessing electrochemical performances of *in situ* diffuse reflectance spectroelectrochemistry. By combining electrochemistry with diffuse reflectance spectroscopy, this work made an effective complementary for spectroelectrochemistry.

Keywords: Lithium-ion battery; Diffuse reflectance spectroelectrochemistry; *In situ*; Cathode material

1. Introduction

In recent years, there has been a rapid increase in the demand for electric vehicles, thus the requirement for batteries also grows dramatically [1]. Therefore, great efforts have been made in developing new battery systems and optimizing existing battery systems [2]. Improving the performance of batteries relies on accurate evaluation of electrochemical performance of electrode materials inside the batteries. Various characterization techniques have been developed and applied to the studies on electrode materials [3,4]. Among all these techniques, *in situ* methods are particularly favored. Compared to well-established *ex situ* methods, *in situ* methods enable measurements without disassembling the batteries and even while the batteries are functioning under real working conditions [5]. This largely prevents the possible misleading caused by the lack of original chemical environments.

To evaluate the electrochemical performance of electrode materials under working conditions, electrochemical techniques such as cyclic voltammetry (CV) [6], galvanostatic charge/discharge (GCD) [7], and electrochemical impedance

Received 29 December 2023; Received in revised form 26 January 2024; Accepted 21 February 2024
Available online 23 February 2024

* Corresponding author, Hao-Ran Li, Tel: (86-25)89682304, E-mail address: lihaoran@smail.nju.edu.cn.
* Corresponding author, Wei Wang, Tel: (86-25)89680309, E-mail address: wei.wang@nju.edu.cn.

https://doi.org/10.61558/2993-074X.3446

spectroscopy (EIS) [8] are generally adopted. Based on these electrochemical methods, by combining the electrochemistry with the spectroscopy together, a field known as spectroelectrochemistry [9] has been developed. These methods, such as infrared spectroelectrochemistry (IR-SEC), Raman spectroelectrochemistry (Raman-SEC) [10], have been proven to be effective on studying electrode materials and interfacial processes. While these methods are powerful and have been devoting the battery industry with a number of considerable discoveries, their high requirement on advanced detectors, and instrumental modifications that are possible only in specialized labs have limited their applications to a wider range. Despite the great success in IR-SEC and Raman-SEC, there are still some fundamental spectroscopic techniques that have been underused. One example among them is ultraviolet-visible (UV-Vis) spectroscopy, and recently, it has been used to distinguish battery-type, pseudocapacitive and electrical double-layer charge storage processes [11]. Another example is the diffuse reflectance spectroscopy (DRS) [12]. As a spectroscopic method, DRS also reveals the information of chemical species changing during electrochemical reactions, and it has been utilized to study electrode materials [13,14]. It offers a rapid and non-destructive testing that requires little additional sample preparation with simple and straightforward optical setups. These advantages make it suitable to be combined with *in situ* electrochemical measurements.

In the present work, we proposed a specially designed battery based on the structure of coin cells [15] that enables *in situ* DRS measurements during charging and discharging. Since LIBs are the most widely used type of batteries [16,17], and the performance of cathode materials majorly affects the entire batteries, this work took three types of cathode materials that are commonly used in LIBs [18−20] as examples. With the battery mentioned above, *in situ* diffuse reflectance spectroelectrochemistry (DRS-SEC) measurements for half-cell systems carrying LFP, NCM811 and LCO as working electrodes were carried out. By monitoring the spectral changes during charging and discharging in real time, differences of the wavelength under which materials exhibited the greatest changes on optical intensity were quantitively revealed. This could provide guidance for the wavelength selection of the detection light for other kinds of spectroelectrochemistry measurements. Furthermore, by analyzing the spectra under different states of charge (SOC), various spectral features on different materials were extracted and their correlation to batteries responses is discussed. It was anticipated that DRS-SEC could be an effective way to study electrode materials under working conditions in real time, which holds potential for evaluating the performance of electrode materials and revealing mechanisms of electrochemical processes.

2. Experimental section

2.1. Materials and reagents

All cathode materials used as the working electrode were purchased from Guangdong Canrd New Energy Technology Co., Ltd. The electrolyte was 1 $mol \cdot L^{-1}$ $LiPF_6$ in DMC:EC (1:1 v/v). Glass coated with 100 nm copper was used as the current collector of the specially designed batteries. Such conductive and transparent glass was fabricated with magnetron sputtering system (PVD75 Proline SP, Kurt J. Lesker). The specially designed battery shells were fabricated by local manufacturers. All batteries were assembled in a glovebox filled with high-purity argon (Ar) gas ($\geq$99.99%).

2.2. Optical setup and electrochemical measurement

The optical system of dark-field microscopy was performed on an orthoptic microscopy (Nikon, eclipse LV-N) equipped with a 20× objective (numerical aperture = 0.4, working distance = 19 mm). The light source was reflected by a beam splitter, then the well-focused spot passed through the objective lens and irradiated on the cathode materials across the optical window of the specially designed batteries. Finally, the reaction beam was reflected upward and collected by the camera. The laser beam in the spectral calibration experiments was provided by NKT Photonics. In the DRS experiments of three types of electrode materials, halogen lamp was selected as the light source. The spectrograph (spectral range: 400−1000 nm) was purchased from Specim and was connected directly to the microscopy as a module. A CCD camera (Manta G-917B, AVT) with an ultra-large format (3384 × 2710 pixels, 3.69 μm/pixel) was used to record time-lapsed images of spectra. All GCD experiments of half-cells were performed with a potentiostat (CHI760e, CH Instruments, Inc.). A standard half-cell structure, where fresh lithium served as the reference and counter electrodes, and cathode materials served as the working electrode, was employed in all GCD experiments.

3. Results and discussion

3.1. Realizing in situ diffuse reflectance spectra measurements

Figure 1a schematically illustrates the experimental apparatus, which consists of an up-right

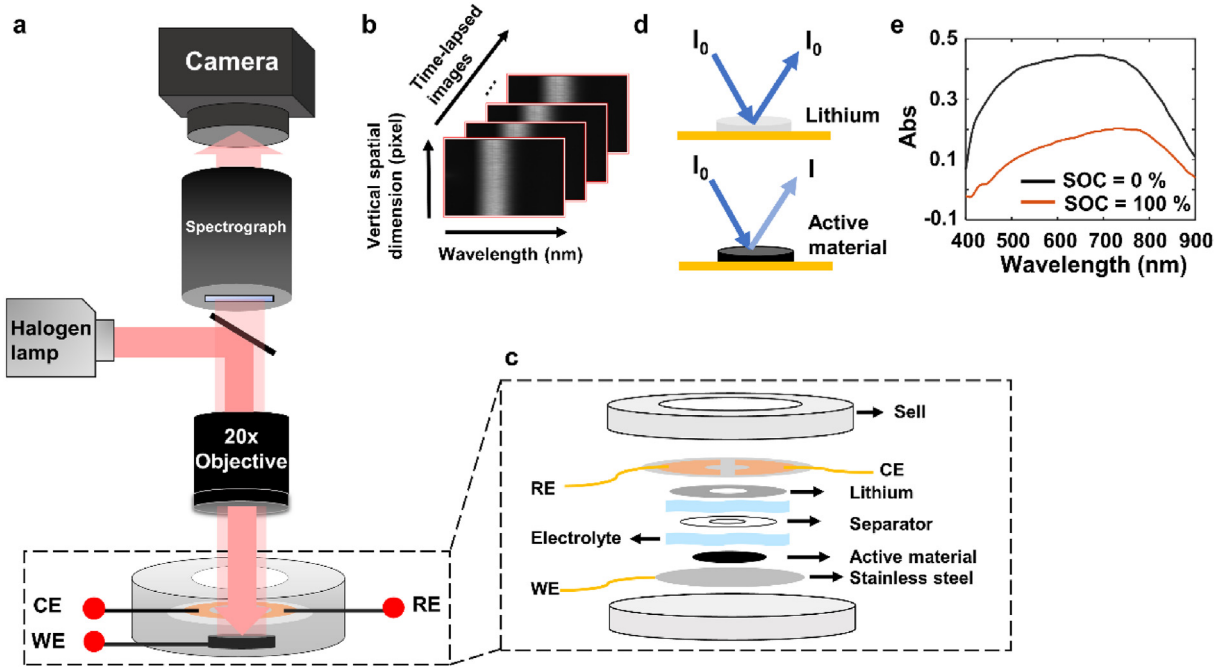

Fig. 1. (a) Schematic illustration of the experimental apparatus. (b) Raw spectral images obtained from the camera through the spectrograph. (c) Detailed illustration of the battery structure used in the experiments. (d) Schematic diagram showing how the intensities of the incident light (I_0) and the reflected light (I) are defined. (e) The spectra extracted from spectral images varied with chemical reactions. The black line marks the fully discharged state of LFP (SOC = 0%) and the red line stands for the fully charged state (SOC = 100%).

dark-field microscopy [21] for recording spectral changes, a spectrograph, and a specially designed battery for observing cathode materials in real time. Halogen lamp was used as the light source because it provided a bright white illumination with good continuity. The light source was reflected upward into the camera through the spectrograph, and the camera collected a series of time-lapsed images as shown in Fig. 1b.

In order to observe electrode materials during the electrode reaction processes, a half-cell based on the structure of coin cells with a transparent window was constructed. A half-cell structure was employed because this work aimed to study cathode materials. In the half-cells, fresh metal lithium worked as the reference electrode and counter electrode, while cathode materials worked as the working electrodes. The specific structure of the half-cell is shown in Fig. 1c. First of all, a special donut-shaped mold was fixed to a circular glass (diameter = 4 cm), and then this combination was coated with copper. By doing so, the glass was copper-coated everywhere but the mold by magnetron sputtering coater, so a smaller circle in the center of glass (diameter = 0.5 cm) remained transparent (without copper). It was equivalent to open an optical window for the half-cell. Next, the fresh metal lithium, separator, and cathode materials were put under the conductive glass respectively, which were all in a round shape. In order to observe the cathode materials, the centers of the metal lithium and the separator were both perforated. Thus, the cathode materials were able to be monitored with light. Cathode electrodes in this half-cell needed no special treatments. This means that both homemade and commercially available cathode electrodes can be kept in a good working condition. Finally, the fresh metal lithium was in contact with the conductive glass which served as the negative current collector, and cathode electrodes were attached to the stainless-steel plate to ensure that a conductive circuit was formed inside the battery. The both sides of the conductive glass and stainless-steel plate were all bound with conductive tapes to connect the potentiostat. The shells made of anodic aluminum alloy were secured with countersunk screws and the half-cells were all assembled in an Ar-filled glovebox.

As shown in Fig. 1d, the fresh lithium was selected as the reference in the half-cell system. In contrast with the cathode materials, the fresh lithium with nearly white color was considered to absorb little visible light. When the light source irradiated on the lithium, the optical intensities of the reflected light and incident light could be considered as equivalent. On the contrary, the testing cathode materials which were black in color should absorb the visble light. Hence, the reflected light intensity was less than the incident light intensity. To quantify the light that is absorbed by

the materials, the absorbance of cathode materials is calculated by the following equation:

$$Abs = \log_{10}\frac{I_0}{I} \quad (1)$$

where I_0 and I represent the optical intensity of incident light and the optical intensity of reflected light, respectively. Since the structural changes of the cathode materials caused the changes of their refractive index during reaction processes, I varied continuously and thus led to the spectral alteration through reactions. And for the same type of cathode material, the thickness that light travelled through the sample may be considered as the same, so the optical paths are not discussed in this work. Fig. 1e shows spectra under different SOC. When the half-cells are fully charged, their SOC values are defined as 1, *i.e.*, SOC = 100% [22]. On the contrary, SOC = 0% when batteries are fully discharged.

The combination of the spectrograph and the camera was calibrated by acquiring spectral images of the laser at different wavelengths. Lasers at 540, 660, 800 and 900 nm, were selected as the light source and irradiated the fresh lithium respectively. The raw spectral images collected from the camera are shown in Fig. 2a. Every spectral image consisted of 3384 × 338 pixels because the images were processed with binning in the y-direction to enhance the signal-to-noise ratio (SNR). Vertical axis of every spectral image represented the spatial distribution of the sample site, while horizontal axis stood for wavelengths. Then four optical intensity curves of four lasers at different wavelengths were obtained, which were from the vertical spatial distributions of spectral images. Optical curves were all normalized in order to show the correspondence between optical intensity and pixel position, as shown in Fig. 2b (red dashed lines). Pixel position of spectral center with every wavelength was obtained by Gaussian-fitting with ordinary least square regression (blue lines). It can be seen that wavelengths had a good linear relationship with pixels (Fig. 2c), so every pixel of spectral images corresponded to one slim band of wavelength.

3.2. Guiding wavelength selection of detection light for different materials

Three commercially available cathode electrodes in LIBs were assembled respectively into half-cells, and were tested by GCD at 1C. Commercially available cathode electrodes have uniform distribution of active particles and are therefore suitable to be used to study spectra of whole electrode. Here, $LiFePO_4$ half-cell was taken as an example (NCM811 and LCO were the same in terms of lithiation and delithiation mechanisms), its charging and discharging reactions were expressed as:

$$LiFePO_4 - xLi^+ - xe^- = xFePO_4 + (1-x)LiFePO_4 \quad (2)$$

$$FePO_4 + xLi^+ + xe^- = xLiFePO_4 + (1-x)FePO_4 \quad (3)$$

The charging and discharging processes of LFP were actually the lithiation and delithiation processes. In the charging process (oxidation reaction), lithium-ion came out from the lattice of LFP

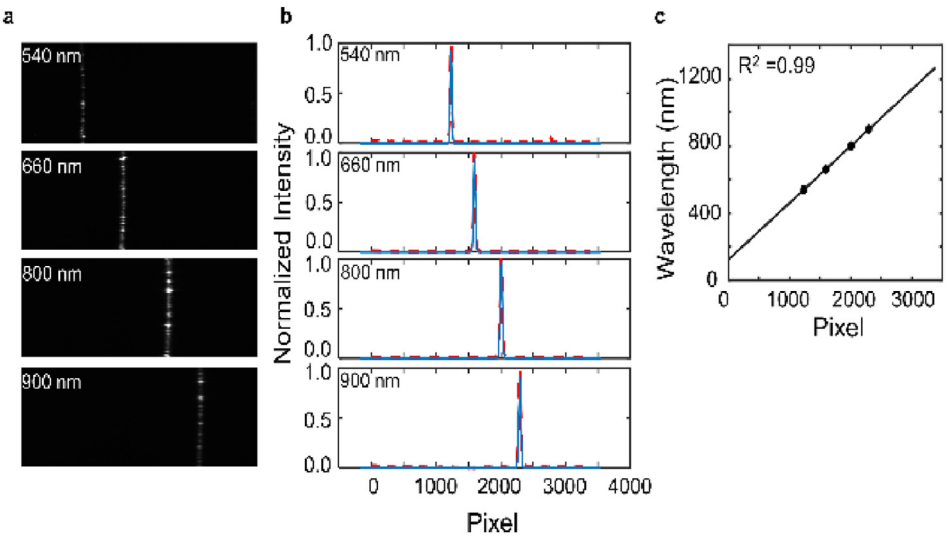

Fig. 2. (a) Spectral images of laser at different wavelengths. (b) Optical intensity extracted from the spectral images on the left. Experimental data (red dashed lines) was obtained by irradiating the reference with lasers at different wavelengths. The center of each spike was obtained by Gaussian-fitting with ordinary least square regression (blue lines). (c) Linear relationship between wavelengths and pixels.

(delithiation reaction), and subsequently crossed the separator through the electrolyte to reach the anode material (which is metal lithium in half-cell systems), as shown in equation (2). While in the discharging process (reduction reaction), conversely, lithium-ion came out from the anode material, crossed the separator to reach the cathode electrode and finally entered into the lattice of LFP (lithiation reaction), as shown in equation (3). After one charge-discharge cycle, lithium-ion moved back and forth between the cathode and anode electrodes to form the so-called "rocking chair battery". Movement of lithium-ion caused structure transformation of cathode materials, which inevitably induced changes of DRS.

Figure 3a, d, g show the real-time DRS data of LFP, NCM811 and LCO, respectively, during charging and discharging. Firstly, it can be seen that DRS curves of these cathode materials are largely different, confirming the authenticity of DRS measured by this *in situ* method. In this way, different types of cathode materials can be identified by DRS. Secondly, DRS responses are changed with different stages of reactions. Fig. 3b, e, h show the typical spectra of LFP, NCM811 and LCO under different SOC conditions. It can be seen that all half-cells had good reversibility through one charge-discharge cycle.

Absorbance range (ΔAbs) is defined as the absorbance difference between the fully charged state and fully discharged state at every single wavelength band. As shown in Fig. 3c, LFP had the largest absorbance range at 515 nm, indicating that LFP would respond most sensitively to the beam at 515 nm. Similarly, when a monochromatic light source at 629 nm is used to irradiate the NCM811, it will have the largest change in optical intensity (Fig. 3f). Upon a light source at 727 nm being chosen to irradiate the LCO, the largest change in optical intensity will be observed (Fig. 3i). As shown above, the absorbance range curves can be used to guide the optimization of monochromatic beam in subsequent studies of each cathode material. By combining electrochemistry with diffuse reflectance spectroscopy, more qualitative and quantitative information about the processes occurring at the cathode electrodes can be obtained.

3.3. Various spectral features exhibiting on different materials

Since the DRS spectra of the cathode materials exhibited broadband and peakless absorption features, the weighted average of wavelength taking absorbance as the weights is employed by the following equation:

$$\text{Weighted average of wavelength} = \frac{\sum \lambda \cdot Abs(\lambda)}{\sum Abs} \quad (4)$$

where λ represents the central wavelength of the wavelength band and $Abs(\lambda)$ is the absorbance

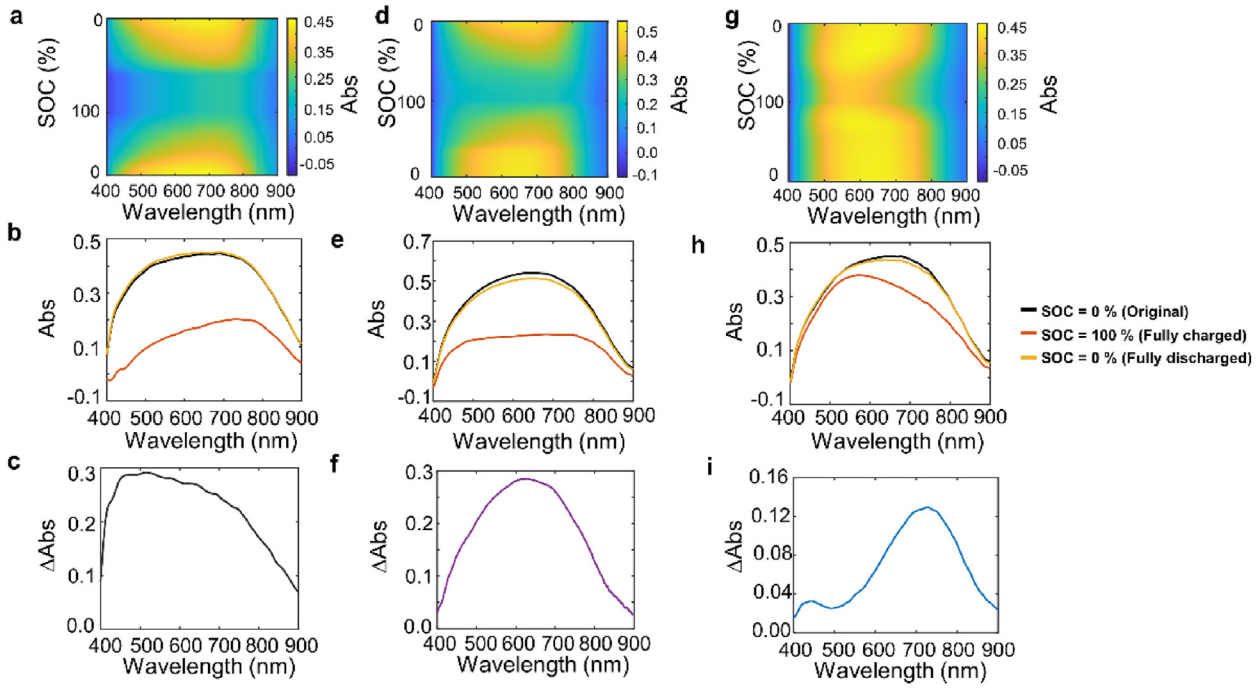

Fig. 3. All DRS curves of (a) LFP, (d) LCO and (g) NCM811 under different SOC conditions during GCD test at 1C; Three typical spectra of (b) LFP, (e) NCM811 and (h) LCO; The corresponding absorbance range curves of (c) LFP, (f) NCM811 and (i) LCO.

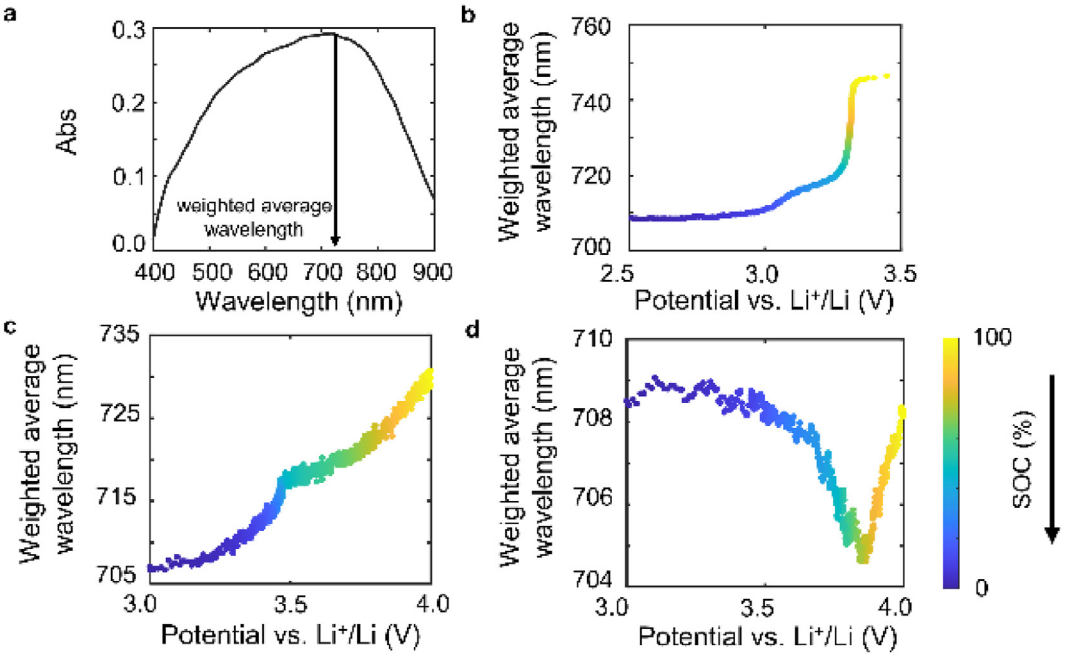

Fig. 4. (a) A typical DRS spectrum and its corresponding weighted average wavelength. The weighted average wavelength changing curves of (b) LFP, (c) NCM811 and (d) LCO under discharging process.

corresponding to the single wavelength band. This makes it possible to extract one wavelength band which can statistically stand for the average energy state of the materials for further analysis. As shown in Fig. 4a, the weighted average wavelength of cathode materials was calculated and is marked. The weighted average wavelength during discharging varied for different cathode materials. In Fig. 4b the weighted average wavelength exhibited a blue shift from 746 nm to 708 nm for LFP. This phenomenon is related to band gap changes of materials during reactions. When the LFP half-cell was totally discharged, $FePO_4$ became $LiFePO_4$, and then its band gap increased. It caused $LiFePO_4$ to absorb more photon energy, thus the spectra were blue-shifted, which was consistent with previous report [23]. In addition, the weighted average wavelength sharply decreased at 3.3 V, which corresponded to the charging platform of LFP and was related to phase transition through the reaction. Similarly, as shown in Fig. 4c, the weighted average wavelength of NCM811 decreased from 730 nm to 707 nm through discharging process. For both LFP and NCM811, the weighted average wavelengths are blue-shifted during lithium process, but LCO showed a different behavior. The weighted average wavelength of LCO firstly decreased from 708 nm to 704 nm, and then turned back to 708 nm at a turning point (3.8 V) where the interfacial phase transition happened. Also, the degree of change for the weighted average wavelength was much smaller than those of LFP and NCM811. To clarify, the cut-off voltages of these three types of cathode materials were determined by their respective material properties.

4. Conclusions

In this work, a specially designed battery was constructed based on the structure of coin cells to visualize spectral changes of cathode materials during reactions. The electrodes in batteries required little treatments, and both homemade and commercially available electrodes can be kept in good working conditions. Accordingly, *in situ* DRS-SEC measurements were carried out with the three types of cathode materials, namely, LFP, NCM811 and LCO, for LIBs, obtaining the real-time absorption spectra of the testing electrode materials. This approach not only provided a simple measurement accessory for diffuse reflectance spectroscopy, but also complemented *in situ* characterization techniques for LIBs. Subsequently, the heterogeneity of different cathode materials on interaction relationships with the lights of different wavelengths was revealed. It was found out that the responses of different electrode materials to visible light of different wavelengths are closedly related under ordinary reflectance illumination conditions. By analyzing the DRS data, the absorbance range curves are proposed to use as guide for the selection of wavelength of monochromatic detection beam for each material in future optical imaging studies. This work

combined electrochemistry with diffuse reflectance spectroscopy, achieving an effective complementary for spectroelectrochemistry.

Acknowledgements

We acknowledge the financial support from the National Natural Science Foundation of China (No. 21925403) and the Excellent Research Program of Nanjing University (Grant No. ZYJH004).

Conflict of interest

The authors decline on competing interest.

References

[1] Degen F, Winter M, Bendig D, Tübke J. Energy consumption of current and future production of lithium-ion and post lithium-ion battery cells[J]. Nat. Energy, 2023, 8(11): 1284−1295.

[2] Zhao L, Hu Y S, Li H, Wang Z X, Xu H X, Huang X J, Chen L Q. Applications of Raman spectroscopy technique in lithium ion batteries[J]. J. Electrochem., 2011, 17(1): 12−23.

[3] Ren B, Li J F, Huang Y F, Zeng Z C, Tian Z Q. Electrochemical surface-enhanced Raman spectroscopy—current status and perspective[J]. J. Electrochem., 2010, 16(3): 305−316.

[4] Li W J, Zheng J Y, Gu L, Li H. Researches on *in-situ* and *ex-situ* characterization techniques in lithium batteries[J]. J. Electrochem., 2015, 21(2): 99−114.

[5] Li H R, Wang W. Recent advances of *in situ* and *in operando* optical imaging techniques for battery researches[J]. Curr. Opin. Electrochem., 2023, 41: 101376.

[6] Elgrishi N, Rountree K J, McCarthy B D, Rountree E S, Eisenhart T T, Dempsey J L. A practical beginner's guide to cyclic voltammetry[J]. J. Chem. Educ., 2018, 95(2): 197−206.

[7] Liu H N, Naqvi I H, Li F J, Liu C L, Shafiei N, Li Y L, Pecht M. An analytical model for the CC-CV charge of Li-ion batteries with application to degradation analysis[J]. J. Energy Storage, 2020, 29: 101342.

[8] Wang J, Huang Q A, Li W H, Wang J, Zhuang Q C, Zhang J J. Fundamentals of distribution of relaxation times for electrochemical impedance spectroscopy[J]. J. Electrochem., 2020, 26(5): 607−627.

[9] Kaim W, Fiedler J. Spectroelectrochemistry: the best of two worlds[J]. Chem. Soc. Rev., 2009, 38(12): 3373−3382.

[10] Lozeman J JA, Führer P, Olthuis W, Odijk M. Spectroelectrochemistry, the future of visualizing electrode processes by hyphenating electrochemistry with spectroscopic techniques[J]. Analyst, 2020, 145(7): 2482−2509.

[11] Zhang D Z, Wang R C, Wang X H, Gogotsi Y. *In situ* monitoring redox processes in energy storage using UV-Vis spectroscopy[J]. Nat. Energy, 2023, 8(6): 567−576.

[12] Edwards P, Zhang C J, Zhang B G, Hong X Q, Nagarajan V K, Yu B, Liu Z W. Smartphone based optical spectrometer for diffusive reflectance spectroscopic measurement of hemoglobin[J]. Sci. Rep., 2017, 7(1): 12224.

[13] Liu H F, Guo B G, Wang L, Xie R S, Yang J C, Li J, Zhang X Q, Zheng K, Huo J C. Adjusting the photoconductive properties of $LaCoO_3$ thin films by epitaxial strain [J]. Opt. Mater., 2021, 121: 111537.

[14] Pandya R, Valzania L, Dorchies F, Xia F, Mc Hugh J, Mathieson A, Tan H J, Parton T G, Godeffroy L, Mazloomian K, Miller T S, Kanoufi F, Volder M D, Tarascon J, Gigan S, Aguiar H B, Grimaud A. Three-dimensional operando optical imaging of particle and electrolyte heterogeneities inside Li-ion batteries[J]. Nat. Nanotechnol., 2023, 18(10): 1185−1194.

[15] Liu Y S, Sun Q, Yang X F, Liang J N, Wang B Q, Koo A, Li R Y, Li J, Sun X L. High-performance and recyclable Al-air coin cells based on eco-friendly chitosan hydrogel membranes[J]. ACS Appl. Mater. Interfaces, 2018, 10(23): 19730−19738.

[16] Xu C J, Dai Q, Gaines L, Hu M M, Tukker A, Steubing B. Future material demand for automotive lithium-based batteries[J]. Commun. Mater., 2020, 1(1): 99.

[17] Barbosa J C, Gonçalves R, Costa C M, Lanceros-Méndez S. Toward sustainable solid polymer electrolytes for lithium-ion batteries[J]. ACS Omega, 2022, 7(17): 14457−14464.

[18] Zhang J N, Li Q H, Ouyang C Y, Yu X Q, Ge M Y, Huang X J, Hu E Y, Ma C, Li S F, Xiao R J, Yang W L, Chu Y, Liu Y J, Yu H G, Yang X Q, Huang X J, Chen L Q, Li H. Trace doping of multiple elements enables stable battery cycling of $LiCoO_2$ at 4.6 V[J]. Nat. Energy, 2019, 4(7): 594−603.

[19] Wang J Y, Wang R, Wang S Q, Wang Y F, Zhan C. Facile one-step solid-state synthesis of Ni-rich layered oxide cathodes for lithium-ion batteries[J]. J. Electrochem., 2022, 28(8): 2112131.

[20] Wei X F, Guan Y B, Zheng X H, Zhu Q Z, Shen J R, Qiao N, Zhou S Q, Xu B. Improvement on high rate performance of $LiFePO_4$ cathodes using graphene as a conductive agent[J]. Appl. Surf. Sci., 2018, 440: 748−754.

[21] Wang W. Imaging the chemical activity of single nanoparticles with optical microscopy[J]. Chem. Soc. Rev., 2018, 47(7): 2485−2508.

[22] Lu J H, Xiong R, Tian J P, Wang C X, Sun F C. Deep learning to estimate lithium-ion battery state of health without additional degradation experiments[J]. Nat. Commun., 2023, 14(1): 2760.

[23] Zhang Y, Alarco J A, Best A S, Snook G A, Talbot P C, Nerkar J Y. Re-evaluation of experimental measurements for the validation of electronic band structure calculations for $LiFePO_4$ and $FePO_4$[J]. RSC Adv., 2019, 9(2): 1134−1146.

锂离子电池正极材料原位漫反射光谱电化学研究

陈露露，李浩冉*，刘维祎，王伟*
生命分析化学国家重点实验室，南京大学化学化工学院，江苏 南京 210023

摘要

发展原位电化学光谱方法对深入研究电化学反应机理，并最终提高电池性能有着重要价值。建立在这一认识之上，能够应用于电池体系的原位光谱电化学表征技术被认为是表征电池电极材料性能的有效方法。但是受限于电池严格密封的不透明外壳和当前商用电池体系严格隔绝水氧的客观要求，开发更贴近真实电池工作条件的原位光谱电化学表征技术仍有较大需求。基于此，本文设计了一种基于传统纽扣电池架构的原位电化学池，该装置通过特殊设计实现了在尽可能模拟电池工作环境的前提下拥有透明的上盖，从而使发生电化学反应的同时进行光学检测成为可能。利用这一电化学池，本文以锂离子电池中常用的正极材料 $LiFePO_4$(LFP)、NCM811 和 $LiCoO_2$(LCO)为例，对其电化学反应过程中的漫反射光谱进行了采集和分析。相关数据定量地揭示了不同种类电极材料在一般反射光路架构下对不同波长可见光的响应关系，并能够直接用于对单色光检测场景下的波长优化提供指导和依据。更进一步，本文还对不同材料在充放电过程中的光谱特征进行了定量分析，揭示了其光谱特征同材料内在能级状态间的相关性。综上，本文提出了一种基于漫反射光谱的原位光谱电化学表征方法，作为对光谱电化学应用于电池体系的有效补充，本方法能够为评估电极材料性能提供一种全新且简单直接的途径，并最终助力电池性能的提升。

关键词：锂离子电池；漫反射光谱电化学；原位；正极材料